Extending the Strong-Coupling Region and Enhancing the Power Conversion Capability of the Conventional Three-Coil Pseudo-Hermitian WPT System by Using Double Receivers

Zhijiang Liang, Lihui Yang, Xianglin Hao, *Student Member, IEEE*, Chaoran Yang, Shiqing Cai, *Student Member, IEEE*, and Xikui Ma

***Abstract*—Pseudo-Hermitian wireless power transfer (WPT) system relaxes the rigid symmetry constraints of the parity-time WPT system. However, with series-compensation coils, the conventional three-coil pseudo-Hermitian WPT system has two limitations. One is that it exhibits a limited transfer efficiency under a low load coefficient. The other is if a full-bridge inverter is used to implement the negative resistance, the system's output power reaches its minimum at the bifurcation point with a maximum transfer efficiency, significantly restricting the system performance. In this article, a novel double-receiver pseudo-Hermitian WPT system incorporating an intermediate coil is proposed. Compared with the conventional system under the same load, the proposed system has two advantages. One is if the load coefficient is low, using double decoupled RXs can extend the strong-coupling region and enhance the steady transfer efficiency. The other is that a well-designed cross-coupling can be leveraged to enhance the power conversion capability, and circumvent the binary choice between the steady transfer efficiency and the output power. Experimental results demonstrate that by using the proposed system with double decoupled RXs, the strong-coupling region can be extended and the steady transfer efficiency can be enhanced. Experimental results also demonstrate that a few times enhancement in the power conversion capability can be achieved by leveraging the cross-coupling between the double RXs.**

***Index Terms*—Double receivers, power conversion capability enhancement, pseudo-Hermitian, steady transfer efficiency enhancement, wireless power transfer (WPT).**

I. Introduction

DUE to the advantages of high reliability and convenience, the wireless power transfer (WPT) technology has developed rapidly. The magnetically coupled resonant (MCR) WPT system was first reported in 2006 [1]. From then on, the rapid development of WPT has facilitated various applications, such as the electric vehicles and biomedical implant devices. However, the traditional WPT system is not robust against the misalignment between the coupling coils and the variation of load, thus limiting the application scenarios of this technology. To enhance the robustness of the system, the methods, such as coupling structure optimization [2], [3], impedance matching network [4], and dual-side control [5], have been proposed in recent years. However, most of these methods suffer from the drawbacks, such as high cost and high complexity.

For example, an adaptive impedance-matching network capacitor matrix is proposed in [4], which can be automatically reconfigured to track the optimal impedance-matching point against the misalignment of the coils. Obviously, this control strategy is complex. A dual-side control strategy is proposed in [5] to improve the transfer efficiency against the variation of the mutual coupling and load. Nevertheless, the wireless communication between the transmitting coil (TX) side and the receiving coil (RX) side is needed for the feedback control, which inevitably increases the overall system cost.

Therefore, a problem arises, i.e., is there any existing method that can provide a simple solution against the variation of mutual coupling and load? The PT symmetry provides a good idea to solve this problem. The concept of parity-time (PT) symmetry is first used to design a robust PT WPT system in 2017 [6]. Within the framework of the coupled mode theory (CMT), the dynamics of the considered WPT system can be characterized as $\mathrm{d}\boldsymbol{a}/\mathrm{d}t = \boldsymbol{H}\boldsymbol{a}$. If the matrix $\boldsymbol{H}$ is invariant under the combined P-reversal and T-reversal, where P-reversal refers to the inversion of space, and T-reversal refers to the inversion of the flow of time [7], then the WPT system is said to be PT-symmetric. For the PT WPT system, the constant output power and constant steady transfer efficiency can be achieved in the PT-symmetric region without any active control or communication. However, they cannot be maintained in the broken PT-symmetric region [6].

To extend the PT-symmetric region, various methods have been proposed in recent years, such as using the intermediate coil (IC) [8], [9], [10], high-order compensation network [11], [12], [13], double-transmitters [14], multiple receivers [15],

Received 21 November 2024; revised 21 February 2025 and 27 April 2025; accepted 26 May 2025. Date of publication 3 June 2025; date of current version 5 August 2025. Recommended for publication by Associate Editor A. Kuperman. *(Corresponding author: Lihui Yang.)*

Zhijiang Liang, Lihui Yang, Chaoran Yang, Shiqing Cai, and Xikui Ma are with the State Key Laboratory of Electrical Insulation and Power Equipment, School of Electrical Engineering, Xi'an Jiaotong University, Xi'an 710049, China (e-mail: zjliang@stu.xjtu.edu.cn; lihui.yang@mail.xjtu.edu.cn; ycr1868@stu.xjtu.edu.cn; caisq1024@stu.xjtu.edu.cn; maxikui@mail.xjtu.edu.cn).

Xianglin Hao is with the Department of Electrical Engineering, City University of Hong Kong, Hong Kong, China (e-mail: xianglhao2-c@my.cityu.edu.hk).

Color versions of one or more figures in this article are available at https://doi.org/10.1109/TPEL.2025.3576189.

Digital Object Identifier 10.1109/TPEL.2025.3576189

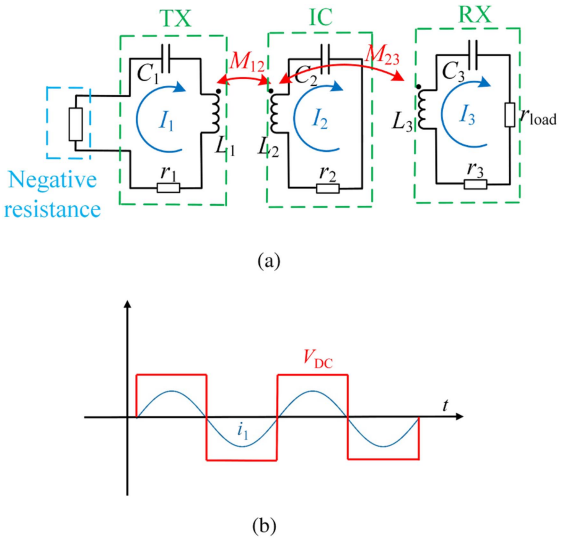

Fig. 1. (a) Schematic diagram of a conventional three-coil pseudo-Hermitian WPT system with a S-S-S configuration. (b) Schematic diagram of a full-bridge inverter-based negative resistance.

[16], ON–OFF key modulation [17] and parallel–parallel configuration [18]. Nevertheless, some rigid limitations are required to ensure that the system is PT-symmetric. For example, for a three-coil WPT system consisting of a TX, an IC and a RX, to ensure that the system is PT-symmetric, the coupling coefficients between the adjacent resonators must be equal [8], [19].

Therefore, another problem arises, i.e., if the system is not PT-symmetric, is there still exists a purely real eigenvalue of the matrix $\boldsymbol{H}$? Fortunately, researchers have found that if there exists an operator η which satisfies $\eta^{\dagger} = \eta$, and at the same time the matrix $\boldsymbol{H}$ satisfies $\boldsymbol{H}^{\dagger} = \eta \boldsymbol{H} \eta^{-1}$ [19], [20], it is said that the system is a pseudo-Hermitian system and there always exists a purely real eigenvalue of the matrix $\boldsymbol{H}$. Obviously, the pseudo-Hermitian WPT system relaxes the rigid requirements of the PT WPT system and has a broader application scenario [19], [21], [22].

Since it is well known that using a three-coil configuration can extend the power transfer distance, a conventional three-coil pseudo-Hermitian WPT system consisting of a TX, an IC and a RX with a parallel–series–parallel configuration is first studied in [19], where an operational amplifier with resistors are used to implement the negative resistance $-R$. However, Hao et al. [19] focused on discussing the eigenmode selection mechanism of the system theoretically. Therefore, it would be useful to discuss the steady transfer performance of the system, where a switching inverter is used to implement the negative resistance $-R$ and under the most commonly used configuration, i.e., the series-series-series (S-S-S) configuration, as shown in Fig. 1.

In this article, the limitations of the conventional three-coil pseudo-Hermitian WPT system with a S-S-S configuration are discussed. Assuming that the positions of TX and IC are both fixed while the position of RX is varied, it is found that one of the limitations is that the evolution of the steady transfer efficiency is limited when the load coefficient of the system is low. The

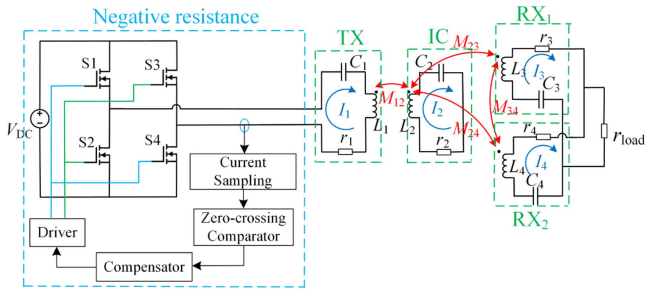

Fig. 2. Schematic diagram of the proposed double-receiver pseudo-Hermitian WPT system incorporating an IC.

other limitation is if a full-bridge inverter is used to implement the negative resistance $-R$, the system's output power reaches its minimum at the bifurcation point with a maximum transfer efficiency, thus significantly restricting the system performance and resulting in a binary choice between the transfer efficiency and the output power.

These two limitations restrict the application scenario of the conventional system. For a middle or long range WPT system with a high operating frequency ω, the reactance ωL of RX is usually large. At this time a low value of load corresponds to a low value of the load coefficient, thus resulting in a limited steady transfer efficiency. In addition, if the power conversion capability of the system is low, usually a boost converter is recommended to raise the input voltage, which will inevitably reduce the dc–dc efficiency and increase the system cost. Solving these limitations will have a practical value in the engineering practice.

To overcome the limitations of the conventional three-coil system with a S-S-S configuration, a novel double-receiver pseudo-Hermitian WPT system incorporating an IC is proposed, as shown in Fig. 2. The double RXs are assumed to be symmetrically placed about the IC. Although a similar structure (i.e., multiple RXs are symmetrically placed about the TX) has been used to improve the transfer performance of a two-coil PT WPT system in [15], it is the first time to use this novel structure in the conventional three-coil pseudo-Hermitian WPT system with a S-S-S configuration to overcome its limitations. The advantages of the proposed system under the same load are given below:

1) The evolution of the steady transfer efficiency of a conventional three-coil system with a S-S-S configuration under a low load coefficient is low. At this time, it is recommended to use double decoupled RXs to double the load coefficient, thus extending the strong-coupling region and enhancing the steady transfer efficiency.
2) The power conversion capability of the conventional system with a S-S-S configuration can be enhanced by properly setting the cross-coupling between the double RXs. This finding can be used to circumvent the binary choice between the steady transfer efficiency and the output power.

The rest of this article is organized as follows. In Section II, the transmission characteristics and the bifurcation behaviour of the proposed double-receiver system are analyzed. In Section III, the transmission characteristics and the bifurcation behavior of

the conventional three-coil system are analyzed. In Section IV, the proposed double-receiver system is compared with the conventional system, and the advantages of using the proposed system are analyzed. In Section V, the experimental setup is introduced and the experiments are performed. The performance of the proposed system and the conventional system are measured under different loads and transfer distances. Experimental results confirm the effectiveness of our work. Finally, Section VI concludes this article.

II. Theoretical Analysis of the Proposed Double-Receiver Pseudo-Hermitian WPT System Incorporating an IC

A. System Modeling and Transmission Characteristics of the Proposed System

In Fig. 2, L_1, L_2, L_3, and L_4 are the self-inductances of the TX, IC and double receivers (RX1 and RX2), respectively. C_1, C_2, C_3, and C_4 are the compensation capacitors, which satisfy $\omega_0 = 1/\sqrt{L_1C_1} = 1/\sqrt{L_2C_2} = 1/\sqrt{L_3C_3} = 1/\sqrt{L_4C_4}$, where ω_0 is the natural resonant frequency of each coil. r_1, r_2, r_3, and r_4 are the ac resistances of TX, IC, RX1 and RX2, respectively. V_{DC} is the input voltage of the full-bridge inverter and r_{load} is the equivalent load. The mutual inductances M_{13} and M_{14} between TX and RX1/RX2 are both ignored. To simplify the derivation, four complex variables $\boldsymbol{a}_1$ to $\boldsymbol{a}_4$ are introduced to derive the CMT model. Their expressions are shown in (1), where $q_{\mathrm{C_n}}$ refers to the charge inside the capacitor C_{n}

$$\boldsymbol{a_n} = \sqrt{\frac{L_{\mathrm{n}}}{2}}\frac{\mathrm{d}q_{\mathrm{C_n}}}{\mathrm{d}t} + \mathrm{j}\sqrt{\frac{1}{2C_{\mathrm{n}}}}q_{\mathrm{C_n}} \quad \mathrm{n} = 1, 2, 3, 4. \tag{1}$$

Since double RXs are assumed to be symmetrically placed about IC (i.e., $L_3 = L_4$, $r_3 = r_4$, $M_{23} = M_{24}$), it can be assumed that $\boldsymbol{a}_3 = \boldsymbol{a}_4$ and the CMT model of the system reads as $\frac{\mathrm{d}\boldsymbol{a}}{\mathrm{d}t} = \boldsymbol{H}\boldsymbol{a}$, where the matrix $\boldsymbol{H}$ is shown in (2) and $\boldsymbol{a} = (\boldsymbol{a}_1, \boldsymbol{a}_2, \boldsymbol{a}_3)^{\mathrm{T}}$

$$\boldsymbol{H} = \begin{bmatrix} \frac{\sqrt{2}V_{\mathrm{DC}}}{\pi\sqrt{L_1}|\boldsymbol{a_1}|} - \Gamma_1 + \mathrm{j}\omega_0 & \frac{1}{2}\mathrm{j}k_{12}\omega_0 & 0 \\ \frac{1}{2}\mathrm{j}k_{12}\omega_0 & \mathrm{j}\omega_0 - \Gamma_2 & -\mathrm{j}k_{23}\omega_0 \\ 0 & -\frac{\mathrm{j}k_{23}\omega_0}{2(1+k_{34})} & \frac{-\Gamma_3+\mathrm{j}\omega_0+\frac{\mathrm{j}}{2}k_{34}\omega_0}{1+k_{34}} \end{bmatrix} \tag{2}$$

where $\Gamma_1 = r_1/(2L_1)$, $\Gamma_2 = r_2/(2L_2)$, $\Gamma_3 = (r_3 + 2r_{\mathrm{load}})/(2L_3)$, $k_{12} = M_{12}/\sqrt{L_1L_2}$, $k_{23} = M_{23}/\sqrt{L_2L_3}$, and $k_{34} = M_{34}/\sqrt{L_3L_4}$.

By separating the real and imaginary parts of $\det(\mathrm{j}\omega_{\mathrm{s}}\boldsymbol{I} - \boldsymbol{H}) = 0$, the expression of $\sqrt{2}V_{\mathrm{DC}}/(\pi\sqrt{L_1}|\boldsymbol{a_1}|\omega_0)$ is shown in (3). $\boldsymbol{H}$ has the eigenfrequencies ω as the solutions of the characteristic equation $c_5(\Delta\omega)^5 + c_4(\Delta\omega)^4 + c_3(\Delta\omega)^3 + c_2(\Delta\omega)^2 + c_1(\Delta\omega) + c_0 = 0$, where c_5, c_4, c_3, c_2, c_1, and c_0 are the coefficients shown in Appendix A and $\Delta\omega = (\omega - \omega_0)/\omega_0$. It can be found that the system always has five eigenmodes. Note that each eigenmode with a purely real eigenfrequency corresponds to a limit cycle.

$$\frac{\sqrt{2}V_{\mathrm{DC}}}{\pi\sqrt{L_1}|\boldsymbol{a_1}|\omega_0} = \Gamma_{10} + \frac{A}{B} \tag{3}$$

where $A = \Gamma_{20}(\Delta\omega)^2(1 + k_{34}) + (\Delta\omega)^2\Gamma_{30} + \frac{1}{2}\Gamma_{20}k_{34}\Delta\omega - \frac{1}{4}k_{12}^2\Gamma_{30}$ and $B = (\Delta\omega)^2(1 + k_{34}) + \frac{1}{2}\Delta\omega k_{34} - \Gamma_{20}\Gamma_{30} - \frac{1}{2}k_{23}^2$. Note that $\Gamma_{10} = \Gamma_1/\omega_0$, $\Gamma_{20} = \Gamma_2/\omega_0$ and $\Gamma_{30} = \Gamma_3/\omega_0$.

If the double RXs are decoupled, this characteristic equation can be simplified as (4), which has five radical solutions read as $\Delta\omega_{\mathrm{s1}} = 0$, $(\Delta\omega_{\mathrm{s2}})^2 = (\Delta\omega_{\mathrm{s3}})^2 = \frac{1}{2}(-b_3 + \sqrt{b_3^2 - 4b_1})$ and $(\Delta\omega_{\mathrm{s4}})^2 = (\Delta\omega_{\mathrm{s5}})^2 = \frac{1}{2}(-b_3 - \sqrt{b_3^2 - 4b_1})$

$$b_5(\Delta\omega)^5 + b_3(\Delta\omega)^3 + b_1(\Delta\omega) = 0 \tag{4}$$

where $b_5 = 1$, $b_3 = -k_{23}^2 - \frac{1}{4}k_{12}^2 + \Gamma_{20}^2 + \Gamma_{30}^2$, $b_1 = \Gamma_{20}^2\Gamma_{30}^2 + k_{23}^2\Gamma_{20}\Gamma_{30} - \frac{1}{4}\Gamma_{30}^2k_{12}^2 + \frac{1}{8}k_{12}^2k_{23}^2 + \frac{1}{4}k_{23}^4$.

If the system stabilizes at an eigenmode with a purely real value of $\Delta\omega$, the relationship between the variables $\boldsymbol{a_1}$, $\boldsymbol{a_2}$, and $\boldsymbol{a_3}$ are shown in (5). Power losses of the TX, IC, RX1, and RX2 read as $P_1 = 2\Gamma_1|\boldsymbol{a_1}|^2$, $P_2 = 2\Gamma_2|\boldsymbol{a_2}|^2$, $P_3 = P_4 = |\boldsymbol{a_3}|^2r_3/L_3$, respectively. The output power of the system reads as $P_{\mathrm{load}} = 4|\boldsymbol{a_3}|^2r_{\mathrm{load}}/L_3$, while the steady transfer efficiency is shown in (6). Note that with a reasonable coil design, the value of r_{load} is always much larger than the ac resistance of the coupled coils, i.e., $r_3 \ll r_{\mathrm{load}}$

$$\begin{aligned} \boldsymbol{a_1} &= \frac{\frac{1}{2}\mathrm{j}k_{12}}{\Gamma_{10} - \frac{\sqrt{2}V_{\mathrm{DC}}}{\pi\sqrt{L_1}|\boldsymbol{a_1}|\omega_0} + \mathrm{j}\Delta\omega}\boldsymbol{a_2} \\ \boldsymbol{a_3} &= \frac{-\frac{1}{2}\mathrm{j}k_{23}}{\Gamma_{30} + \frac{1}{2}\mathrm{j}k_{34} + \mathrm{j}\Delta\omega(1 + k_{34})}\boldsymbol{a_2} \end{aligned} \tag{5}$$

$$\begin{aligned} \eta &= \frac{\frac{2|\boldsymbol{a_3}|^2}{L_3}r_{\mathrm{load}}}{\Gamma_1|\boldsymbol{a_1}|^2 + \Gamma_2|\boldsymbol{a_2}|^2 + \frac{|\boldsymbol{a_3}|^2r_3}{L_3} + \frac{2|\boldsymbol{a_3}|^2}{L_3}r_{\mathrm{load}}} \\ &\approx \frac{\Gamma_{30}|\boldsymbol{a_3}|^2}{\Gamma_{10}|\boldsymbol{a_1}|^2 + \Gamma_{20}|\boldsymbol{a_2}|^2 + \Gamma_{30}|\boldsymbol{a_3}|^2}. \end{aligned} \tag{6}$$

Since $\Gamma_{10} = r_1/(2\omega_0L_1)$, $\Gamma_{20} = r_2/(2\omega_0L_2)$, and $\Gamma_{30} = (r_3 + 2r_{\mathrm{load}})/(2\omega_0L_3)$, thus inspiring by [19], we can define $r_1/(2\omega_0L_1)$, $r_2/(2\omega_0L_2)$, and $r_3/(2\omega_0L_3)$ as the loss coefficient of each resonator and define $2r_{\mathrm{load}}/(2\omega_0L_3)$ as the load coefficient of the proposed system.

B. Bifurcation Behavior Analysis of the Proposed System

Here, by using the Floquet theory with the Filippov method [23], [24], the bifurcation behavior of the proposed system is discussed under the following two situations.

1) Zero-Cross-Coupling Between the Double RXs: If the double RXs are decoupled, the transfer region can be classified into the region (i), region (ii) and region (iii). In the region (i), only two stable eigenmodes corresponding to $\Delta\omega_{\mathrm{s2}}$ and $\Delta\omega_{\mathrm{s3}}$ coexist simultaneously. In the region (ii), three stable eigenmodes corresponding to $\Delta\omega_{\mathrm{s1}}$, $\Delta\omega_{\mathrm{s2}}$ and $\Delta\omega_{\mathrm{s3}}$ coexist simultaneously. In the region (iii), only one stable eigenmode corresponding to $\Delta\omega_{\mathrm{s1}}$ exists.

In the region (i), the system will stabilize at one of the two stable eigenmodes with the same steady transfer efficiency. With the increase of k_{23}, the steady transfer efficiency of the system will increase. In the region (ii), three stable eigenmodes coexist simultaneously and the eigenmode corresponding to $\Delta\omega_{\mathrm{s1}}$ has the highest corresponding steady transfer efficiency. Thus it

TABLE I
PARAMETERS OF THE PROPOSED DOUBLE -RECEIVER SYSTEM USED IN SIMULATION AND EXPERIMENT

Parameters	TX	IC	RX1	RX2
$L(\mu\text{H})$	40.45	40.24	38.15	38.18
$C(\text{nF})$	0.626	0.629	0.664	0.663
$r(\Omega)$	0.63	0.63	0.62	0.61
Parameters	C_1	C_2	C_3	C_4
ESR(Ω)	0.08	0.12	0.10	0.10
Parameters	k_{12}	ω_0		
	0.0875	1MHz		

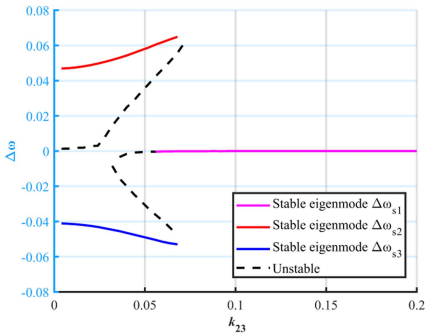

(a)

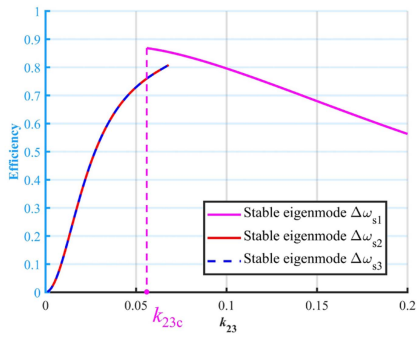

(b)

Fig. 3. (a) Bifurcation diagram of the proposed system with double decoupled RXs and a 5Ω load. (b) Evolution of the steady transfer efficiency corresponding to each stable eigenmode. It should be noted that each spot shown in (a) corresponds to a purely real eigenfrequency, whether the spot is solid or not.

would be useful to ensure that this eigenmode can be selected. In the region (iii), with the increase of k_{23}, the steady transfer efficiency of the system will decrease.

Let ω_{ini} denote the initial operating frequency of the system within the start-up strategy. It is well-known that if multiple eigenmodes coexist simultaneously, the selected eigenmode of the system is dependent on the value of ω_{ini}. Here, ω_{ini} is assumed to be properly set to ensure that the selected eigenmode corresponds to the highest steady transfer efficiency.

Let r_{load} equal to 5Ω for an example, while the other parameters are shown in Table I. Note that the abbreviation ESR refers to the equivalent series resistance of the compensation capacitor. With the help of the Floquet theory with the Filippov method, the bifurcation diagram of the system is shown in Fig. 3(a). With the increase of k_{23}, a bifurcation will occur at the critical coupling

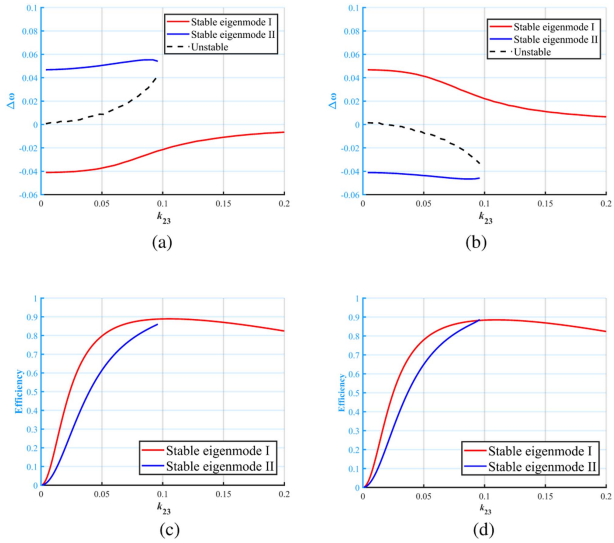

(a) (b) (c) (d)

Fig. 4. (a) and (b) Bifurcation diagram of the proposed system under different values of k_{34}. (c) and (d) Evolution of the steady transfer efficiency corresponding to each stable eigenmode of the proposed system under different values of k_{34}. It should be noted that each spot shown in (a) and (b) corresponds to a purely real eigenfrequency, whether the spot is solid or not. $r_{\text{load}} = 20\Omega$. (a) $k_{34} = 0.15$. (b) $k_{34} = -0.15$. (c) $k_{34} = 0.15$. (d) $k_{34} = -0.15$.

coefficient k_{23c}. The evolution of the steady transfer efficiency corresponding to each stable eigenmode is shown in Fig. 3(b).

2) Nonzero-Cross-Coupling Between the Double RXs: Since the cross-coupling between the double RXs can enhance or weaken each other, the definition of the coupling coefficient k_{34} is extended from $0 \sim 1$ to $-1 \sim 1$ [25]. For the proposed double-receiver system with a nonzero value of k_{34}, the whole transfer region can be classified into the region (i) and region (ii). In the region (i), two stable eigenmodes coexist simultaneously. One of them has a corresponding $\Delta\omega > 0$, while the other has a corresponding $\Delta\omega < 0$. In the region (ii), only one stable eigenmode exists. The stable eigenmode has a corresponding $\Delta\omega < 0$ if $k_{34} > 0$, while it has a corresponding $\Delta\omega > 0$ if $k_{34} < 0$.

In the region (i), if $k_{34} > 0$, the eigenmode corresponding to $\Delta\omega < 0$ has a higher steady transfer efficiency. While if $k_{34} < 0$, at this time the eigenmode corresponding to $\Delta\omega > 0$ has a higher steady transfer efficiency. When two stable eigenmodes coexist simultaneously, a higher steady transfer efficiency can be achieved under a proper ω_{ini}.

For example, let r_{load} equal to 20Ω, $k_{34} = 0.15/-0.15$, while the other parameters of the system are shown in Table I. With the help of the Floquet theory with the Filippov method, the bifurcation diagram of the system is shown in Fig. 4(a) and (b), respectively. The evolution of the steady transfer efficiency corresponding to each stable eigenmode are shown in Fig. 4(c) and (d), respectively. The theoretical results shown in Fig. 4 have verified our conclusions.

Compared with the proposed double-receiver system with zero cross-coupling, under the same load, the cross-coupling between double RXs will lower the steady transfer efficiency, as shown in Fig. 5. Since there is no a general mathematical formula for solving the radical solutions of a quintic equation

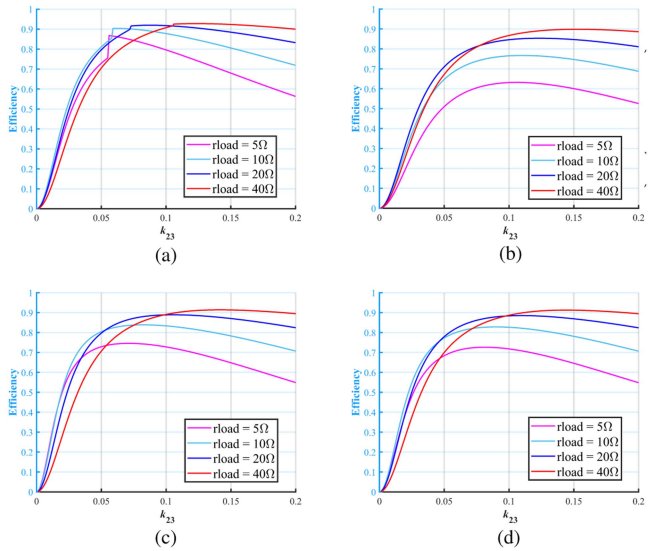

Fig. 5. Evolution of the steady transfer efficiency of the proposed system with different values of k_{34} under different loads. (a) $k_{34}=0$. (b) $k_{34}=0.25$. (c) $k_{34}=0.15$. (d) $k_{34}=-0.15$.

with one unknown $\Delta\omega$, a huge amount of numerical simulation is used.

III. Theoretical Analysis of the Conventional Three-Coil Pseudo-Hermitian WPT System

A. System Modeling and Transmission Characteristics of the Conventional System

The schematic diagram of the conventional system is shown in Fig. 1(a). Similarly, the mutual inductance M_{13} between TX and single RX is ignored. The CMT model of the conventional system reads as $\frac{\mathrm{d}\boldsymbol{a}}{\mathrm{d}t}=\boldsymbol{H}_c\boldsymbol{a}$, where $\boldsymbol{H}_c$ is shown as follows:

$$\boldsymbol{H}_c=\begin{bmatrix}\frac{\sqrt{2}V_{\mathrm{DC}}}{\pi\sqrt{L_1}|\boldsymbol{a_1}|}-\gamma_1+\mathrm{j}\omega_0 & \frac{1}{2}\mathrm{j}k_{12}\omega_0 & 0\\ \frac{1}{2}\mathrm{j}k_{12}\omega_0 & \mathrm{j}\omega_0-\gamma_2 & -\frac{1}{2}\mathrm{j}k_{23}\omega_0\\ 0 & -\frac{1}{2}\mathrm{j}k_{23}\omega_0 & -\gamma_3+\mathrm{j}\omega_0\end{bmatrix} \tag{7}$$

where $\gamma_1=r_1/(2L_1)$, $\gamma_2=r_2/(2L_2)$, and $\gamma_3=(r_3+r_{\mathrm{load}})/(2L_3)$.

By separating the real and imaginary parts of $\det(\mathrm{j}\omega_{\mathrm{s}}\boldsymbol{I}-\boldsymbol{H_c})=0$, the expression of $\sqrt{2}V_{\mathrm{DC}}/(\pi\sqrt{L_1}|\boldsymbol{a_1}|\omega_0)$ is shown in (8). $\boldsymbol{H}_{\mathrm{c}}$ has the eigenfrequencies ω_{S} as the solutions of the characteristic equation (9), which has the radical solutions read as $\Delta\omega_{\mathrm{S1}}=0$, $(\Delta\omega_{\mathrm{S2}})^2=(\Delta\omega_{\mathrm{S3}})^2=\frac{1}{2}(-B_3+\sqrt{B_3^2-4B_1})$, and $(\Delta\omega_{\mathrm{S4}})^2=(\Delta\omega_{\mathrm{S5}})^2=\frac{1}{2}(-B_3-\sqrt{B_3^2-4B_1})$, where $\Delta\omega=(\omega-\omega_0)/\omega_0$.

If the system stabilizes at an eigenmode with a purely real value of $\Delta\omega$, the relationship between the variables $\boldsymbol{a_1}$, $\boldsymbol{a_2}$ and $\boldsymbol{a_3}$ is shown in (10). The output power of the system reads as $P_{\mathrm{load}}=|\boldsymbol{a_3}|^2r_{\mathrm{load}}/2L_3$, while the steady transfer efficiency of the system is shown in (11).

$$\frac{\sqrt{2}V_{\mathrm{DC}}}{\pi\sqrt{L_1}|\boldsymbol{a_1}|\omega_0}=\gamma_{10}+\frac{A_{\mathrm{c}}}{B_{\mathrm{c}}} \tag{8}$$

TABLE II
Parameters of the Conventional Three-Coil System Used in Simulation and Experiment

Parameters	TX	IC	Single RX
$L(\mu\mathrm{H})$	40.45	40.24	38.15
$C(\mathrm{nF})$	0.626	0.629	0.664
$R(\Omega)$	0.63	0.63	0.62
Parameters	C_1	C_2	C_3
ESR(Ω)	0.08	0.12	0.10
Parameters	k_{12}	ω_0	
	0.0875	1MHz	

where $A_{\mathrm{c}}=(\gamma_{20}+\gamma_{30})(\Delta\omega)^2-\frac{1}{4}k_{12}^2\gamma_{30}$ and $B_{\mathrm{c}}=(\Delta\omega)^2-\gamma_{20}\gamma_{30}-\frac{1}{4}k_{23}^2$. Note that $\gamma_{10}=r_1/(2\omega_0L_1)$, $\gamma_{20}=r_2/(2\omega_0L_2)$ and $\gamma_{30}=(r_3+r_{\mathrm{load}})/(2\omega_0L_3)$

$$B_5(\Delta\omega)^5+B_3(\Delta\omega)^3+B_1(\Delta\omega)=0 \tag{9}$$

where $B_5=1$, $B_3=-\frac{1}{2}k_{23}^2-\frac{1}{4}k_{12}^2+\gamma_{20}^2+\gamma_{30}^2$, and $B_1=\gamma_{20}^2\gamma_{30}^2+\frac{1}{2}k_{23}^2\gamma_{20}\gamma_{30}+\frac{1}{16}k_{12}^2k_{23}^2+\frac{1}{16}k_{23}^4-\frac{1}{4}k_{12}^2\gamma_{30}^2$

$$\begin{aligned}\boldsymbol{a_1}&=\frac{\frac{1}{2}\mathrm{j}k_{12}}{\gamma_{10}-\frac{\sqrt{2}V_{\mathrm{DC}}}{\pi\sqrt{L_1}|\boldsymbol{a_1}|\omega_0}+\mathrm{j}\Delta\omega}\boldsymbol{a_2}\\ \boldsymbol{a_3}&=\frac{-\frac{1}{2}\mathrm{j}k_{23}}{\gamma_{30}+\mathrm{j}\Delta\omega}\boldsymbol{a_2}\end{aligned} \tag{10}$$

$$\begin{aligned}\eta&=\frac{\frac{|\boldsymbol{a_3}|^2}{2L_3}r_{\mathrm{load}}}{\gamma_1|\boldsymbol{a_1}|^2+\gamma_2|\boldsymbol{a_2}|^2+\frac{|\boldsymbol{a_3}|^2r_3}{2L_3}+\frac{|\boldsymbol{a_3}|^2}{2L_3}r_{\mathrm{load}}}\\ &\approx\frac{\gamma_{30}|\boldsymbol{a_3}|^2}{\gamma_{10}|\boldsymbol{a_1}|^2+\gamma_{20}|\boldsymbol{a_2}|^2+\gamma_{30}|\boldsymbol{a_3}|^2}.\end{aligned} \tag{11}$$

Since $\gamma_{10}=r_1/(2\omega_0L_1)$, $\gamma_{20}=r_2/(2\omega_0L_2)$, and $\gamma_{30}=(r_3+r_{\mathrm{load}})/(2\omega_0L_3)$, thus inspiring by [19], we can define $r_1/(2\omega_0L_1)$, $r_2/(2\omega_0L_2)$, and $r_3/(2\omega_0L_3)$ as the loss coefficient of each resonator and define $r_{\mathrm{load}}/(2\omega_0L_3)$ as the load coefficient of the conventional system.

B. Bifurcation Behavior Analysis of the Conventional System

For the conventional three-coil system, the bifurcation diagram is similar to the proposed system with double decoupled RXs. The whole transfer region can be classified into the region (i), region (ii) and region (iii). In the region (i), only two stable eigenmodes corresponding to $\Delta\omega_{\mathrm{S2}}$ and $\Delta\omega_{\mathrm{S3}}$ coexist with the same corresponding steady transfer efficiency. With the increase of k_{23}, the steady transfer efficiency will increase.

In the region (ii), three stable eigenmodes coexist simultaneously and the eigenmode corresponding to $\Delta\omega_{\mathrm{S1}}$ has the highest corresponding steady transfer efficiency. While in the region (iii), only one stable eigenmode corresponding to $\Delta\omega_{\mathrm{S1}}$ exist. With the increase of k_{23}, the steady transfer efficiency will decrease.

For example, let r_{load} equal to 5Ω, while the other parameters are shown in Table II. With the help of the Floquet theory with the Filippov method, the bifurcation diagram of the system is shown in Fig. 6(a). The evolution of the steady transfer efficiency corresponding to each stable eigenmode is shown in Fig. 6(b).

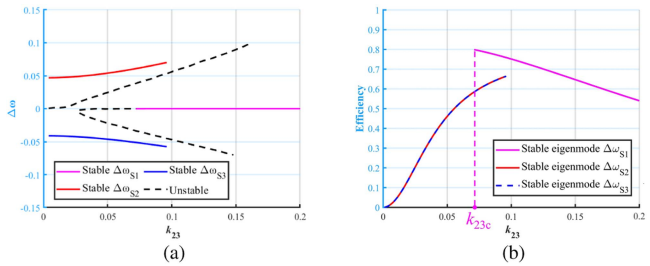

Fig. 6. (a) Bifurcation diagram of the conventional system with a 5Ω load. (b) Evolution of the steady transfer efficiency corresponding to each stable eigenmode. Each spot shown in (a) corresponds to a purely real eigenfrequency, whether the spot is solid or not.

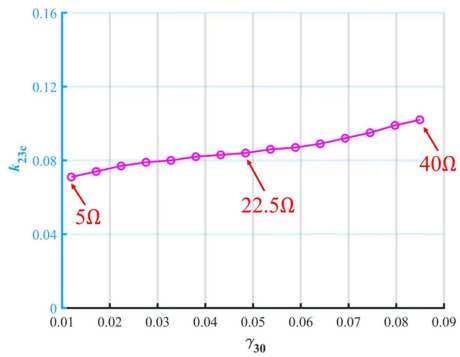

Fig. 7. Evolution of the critical coupling coefficient k_{23c} as a function of γ_{30}. The initial operating frequency $\omega_{\rm ini}$ is set as ω_0.

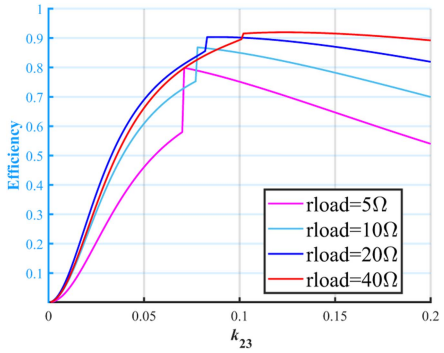

Fig. 8. Evolution of the steady transfer efficiency of the conventional system under different loads. The initial operating frequency $\omega_{\rm ini}$ is set as ω_0.

With the increase of k_{23}, a bifurcation will occur at the critical coupling coefficient k_{23c}.

The evolution of k_{23c} as a function of γ_{30} is shown in Fig. 7. The evolution of the steady transfer efficiency of the system under different loads is shown in Fig. 8. It is obvious that the evolution of the steady transfer efficiency corresponding to the system with a low load coefficient is limited.

IV. Comparing the Transmission Characteristics of the Proposed System With the Conventional System

Here, a comprehensive comparison between the transmission characteristics of the proposed double-receiver system and the conventional three-coil system is made. The advantages of using our proposed system are illustrated in Sections IV-A and IV-B in detail. In addition, the spatial constraint of our proposed system is briefly discussed in Section IV-C.

A. Using Double Decoupled RXs to Extend the Strong-Coupling Region and Enhance the Steady Transfer Efficiency

1) Comparing the Proposed System With the Conventional System Under the Same Load Coefficient and the Same Natural Resonant Frequency ω_0: Let $k_{23\rm s}$ and $k_{23\rm d}$ denote the coupling coefficients k_{23} corresponding to the conventional system and the proposed system, respectively. Comparing the expressions of coefficients b_5, b_3 and b_1 with the expressions of coefficients B_5, B_3, and B_1, and comparing (6) with (11), it is found that if $\gamma_{10}=\Gamma_{10}$, $\gamma_{20}=\Gamma_{20}$ and the coupling coefficient k_{12} of these two systems are all the same, then it is obvious that when $k_{23\rm s}=\sqrt{2}k_{23\rm d}$ and $\gamma_{30}=\Gamma_{30}$, the eigenfrequencies of these two systems are the same. Besides, the steady transfer efficiency corresponding to each pair of the same eigenfrequencies are also the same. In addition, let $k_{23\rm cs}$ and $k_{23\rm cd}$ denote the critical coupling coefficients k_{23c} corresponding to the conventional system and the proposed system, respectively. Since the expressions of $\det(\mathrm{j}\omega_{\rm s}\boldsymbol{I}-\boldsymbol{H})$ and $\det(\mathrm{j}\omega_{\rm s}\boldsymbol{I}-\boldsymbol{H}_c)=0$ are the same at this time, thus it can be concluded that $k_{23\rm cs}=\sqrt{2}k_{23\rm cd}$.

Let $\boldsymbol{a}_{3\rm s}$ and $\boldsymbol{a}_{3\rm d}$ denote the variables $\boldsymbol{a}_3$ corresponding to the conventional system and the proposed system, respectively. Based on the (5) and (10), if $\gamma_{10}=\Gamma_{10}$, $\gamma_{20}=\Gamma_{20}$ and the coupling coefficient k_{12} of these two systems are all the same, then when $k_{23\rm s}=\sqrt{2}k_{23\rm d}$ and $\gamma_{30}=\Gamma_{30}$, it can be concluded that $|\boldsymbol{a}_{3\rm s}|=\sqrt{2}|\boldsymbol{a}_{3\rm d}|$, under the same input voltage $V_{\rm DC}$. Since the output power of the proposed system and the conventional system read as $P_{\rm load}=4|\boldsymbol{a_3}|^2r_{\rm load}/L_3$ and $P_{\rm load}=|\boldsymbol{a_3}|^2r_{\rm load}/(2L_3)$, respectively, we demonstrate that these two systems have the same output power at this time.

2) Comparing the Proposed System With the Conventional System Under the Same Load and the Same Natural Resonant Frequency ω_0: Comparing $\Gamma_{30}=(r_3+2r_{\rm load})/(2\omega_0L_3)$ with $\gamma_{30}=(r_3+r_{\rm load})/(2\omega_0L_3)$, it is found that with the same load, the load coefficient of the proposed system (i.e., $r_{\rm load}/(\omega_0L_3)$) is twice as much as the conventional system (i.e., $r_{\rm load}/(2\omega_0L_3)$). Since $r_3\ll r_{\rm load}$, thus it can be concluded that $\Gamma_{30}=2\gamma_{30}$ under the same load.

In conclusion, for the proposed system with double decoupled RXs and the conventional system, with the same natural resonant frequency ω_0 and the same self-inductance L of each RX, if $\gamma_{10}=\Gamma_{10}$, $\gamma_{20}=\Gamma_{20}$ and the coupling coefficient k_{12} of these two systems are the same, then it can be found that the steady transfer efficiency and power conversion capability of the proposed system with a load R and a value k_{23} of k are the same as the conventional system with a load $2R$ and a value k_{23} of $\sqrt{2}k$, respectively. Two examples have been shown in Fig. 9, while the parameters shown in Tables I and II are used.

3) Advantages About Using Double Decoupled RXs: As shown in Fig. 7, k_{23c} almost remains unchanged when the load coefficient of the conventional system is low. Since the transfer

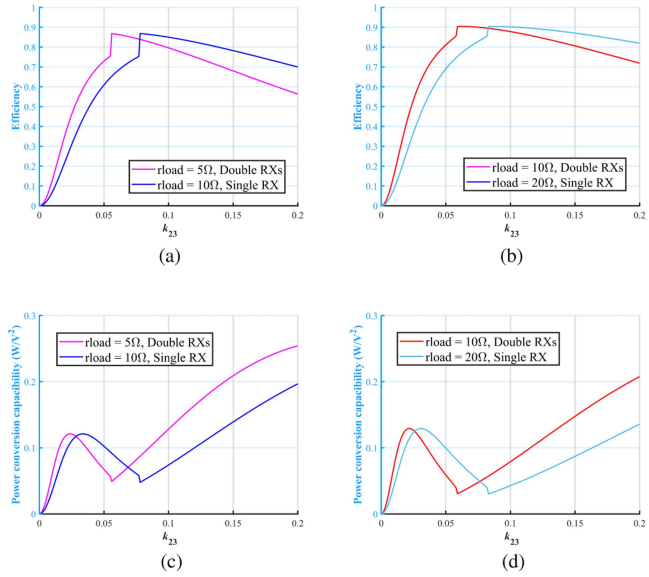

Fig. 9. Evolution of the steady transfer efficiency and power conversion capability of the conventional system and the proposed system under the same load coefficient. (a), (c) $r_{\mathrm{load}} = 5\Omega$, double RXs and $r_{\mathrm{load}} = 10\Omega$, single RX. (b), (d) $r_{\mathrm{load}} = 10\Omega$, double RXs and $r_{\mathrm{load}} = 20\Omega$, single RX. Since the load coefficient of the conventional system and the proposed system are the same, the proposed system with a value k_{23} of k has the same steady transfer efficiency and power conversion capability as the conventional system with a value k_{23} of $\sqrt{2}k$. Note that $k_{34} = 0$ and the initial operating frequency ω_{ini} is set as ω_0.

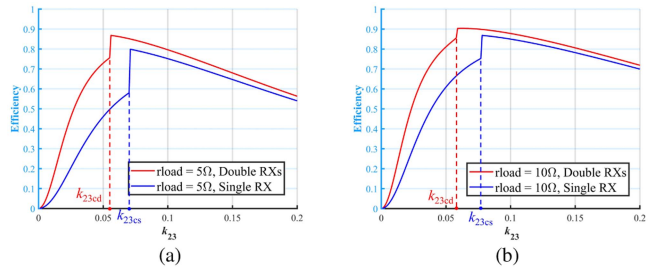

Fig. 10. Using double decoupled RXs to extend the strong-coupling region and enhance the steady transfer efficiency. Note that $k_{34} = 0$ and the initial operating frequency ω_{ini} is set as ω_0. (a) $r_{\mathrm{load}} = 5\Omega$. (b) $r_{\mathrm{load}} = 10\Omega$.

region where $k_{23} > k_{23\mathrm{c}}$ is defined as the strong-coupling region[19], [21], thus it can be concluded that for the conventional system with a low load coefficient, using double decoupled RXs can double the load coefficient and reduce $k_{23\mathrm{c}}$, thus extending the strong-coupling region and enhancing the steady transfer efficiency, as shown in Fig. 10.

More generally, the above conclusions can be extended to the proposed system with multiple decoupled RXs, which are symmetrically placed with an IC. By comparing the characteristic equations of these systems, it can be found that with the same natural resonant frequency ω_0 and the same self-inductance L of each RX, if $\gamma_{10} = \Gamma_{10}$, $\gamma_{20} = \Gamma_{20}$ and the coupling coefficient k_{12} of these two systems are the same, then for the system with n decoupled RXs, the steady transfer efficiency and power conversion capability of the system with a load R and a value

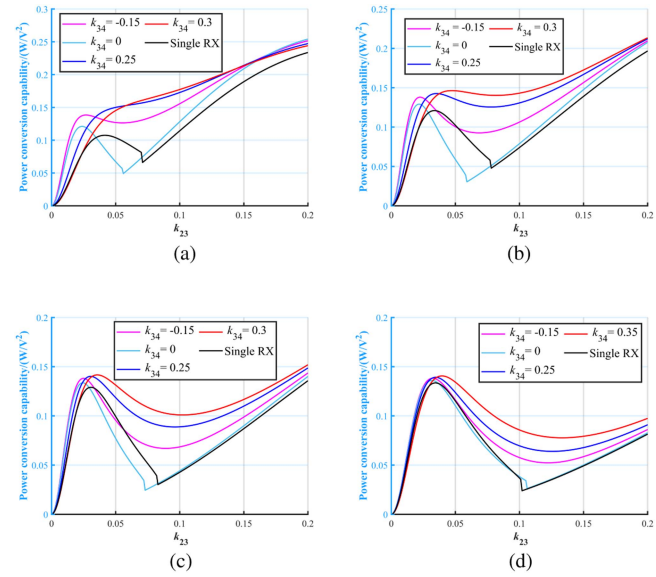

Fig. 11. Evolution of the power conversion capability of the conventional system and the proposed system with different values of k_{34}. (a) $r_{\mathrm{load}} = 5\Omega$. (b) $r_{\mathrm{load}} = 10\Omega$. (c) $r_{\mathrm{load}} = 20\Omega$. (d) $r_{\mathrm{load}} = 40\Omega$.

k_{23} of k are the same as the conventional system with a load nR and a value k_{23} of $\sqrt{n}k$, respectively.

This conclusion is obvious from the physical perspective. To achieve the same output power, the current in each decoupled RX should be $1/\sqrt{n}$ times as the current inside the single RX of the conventional system. If the current inside the IC corresponding to these two systems is the same, at this time the value of $k_{23\mathrm{n}}$ should be equal to $k_{23\mathrm{c}}/\sqrt{n}$. Note that k_{23n} refers to the value of k_{23} corresponding to the system with n decoupled coils.

B. Properly Setting the Cross-Coupling Between the Double RXs to Enhance the Power Conversion Capability

Power conversion capability refers to the ability to achieve a higher output power while the input voltage V_{DC} remains unchanged, which can be defined as (12). For the conventional three-coil system and the proposed system with double decoupled RXs, the power conversion capability achieves a local minimum value at the bifurcation point with a maximum steady transfer efficiency, as shown in Fig. 9. It can be found that the power conversion capability of the system around the bifurcation point is low, resulting in a binary choice between the transfer efficiency and the power conversion capability

$$K = \frac{P_{\mathrm{load}}}{V_{\mathrm{DC}}^2}. \tag{12}$$

As shown in Fig. 11, it can be found that in most cases, using double decoupled RXs cannot enhance the power conversion capability under the same load. Fortunately, by properly setting the cross-coupling between double RXs, the power conversion capability can be enhanced.

Compared with the proposed system with double decoupled RXs, under the same load, the cross-coupling between double RXs will reduce the steady transfer efficiency, thus a tradeoff

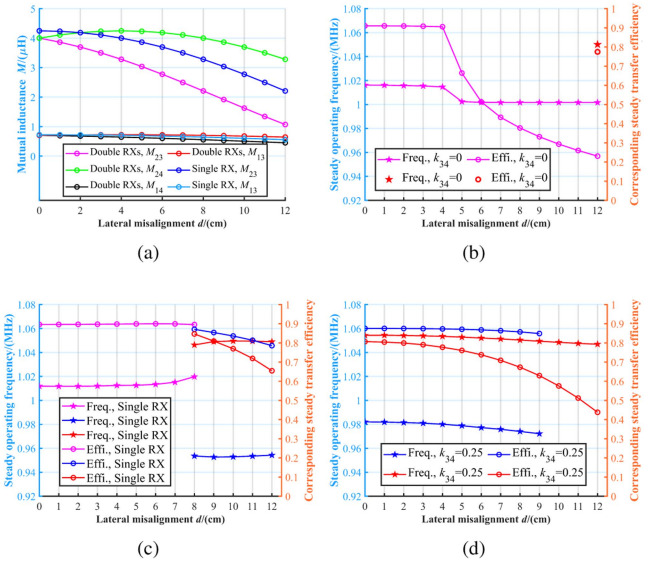

Fig. 12. (a) Evolution of the mutual inductance between the coupling coils. (b)–(d) Evolution of the steady operating frequency and its corresponding steady transfer efficiency, where (b) corresponds to "Double RXs, $k_{34} = 0$", (c) corresponds to "Single RX" and (d) corresponds to "Double RXs, $k_{34} = 0.25$". Note that in (b)–(d), the data with the same color corresponds to each other.

needs to be made. As shown in Fig. 5, it is not recommended to use the cross-coupling between the double RXs to enhance the power conversion capability if the decrease in the steady transfer efficiency is severe.

Based on the above discussion, it can be concluded that a well-designed cross-coupling between the double RXs can be leveraged to enhance the power conversion capability, thus circumventing the binary choice between the steady transfer efficiency and the output power.

C. Negative Influence Caused by the Asymmetric Placement

The perfect symmetry of double RXs may not be achievable in some scenarios. At this time a circulating current in the RX side will occur. Here, the lateral misalignment performance is briefly discussed under the following two situations.

1) Zero-Cross-Coupling Between Double RXs: Let D refers to the center-to-center distance between the IC and RX1/RX2 in the longitudinal direction. Taking the coils shown in Section A, Chapter V as an example. In addition, we assume that r_{load} is selected as 20Ω and D is fixed as 12.5 cm. A conventional three-coil system with the same load is selected as a comparison.

For the proposed double-receiver system, in order to achieve a value k_{34} of 0 or 0.25, the initial center-to-center distance between the IC and RX1/RX2 in the lateral direction should be set as 4 or 3 cm, respectively. For the conventional system, which is used for comparison, this value is set as zero (i.e., IC and single RX are coaxially aligned). Here, Let d refer to the misalignment of the RX side in the lateral direction. With the help of the software COMSOL Multiphysics, the evolution of the mutual inductance between the coupling coils as a function of d can be obtained, as shown in Fig. 12(a).

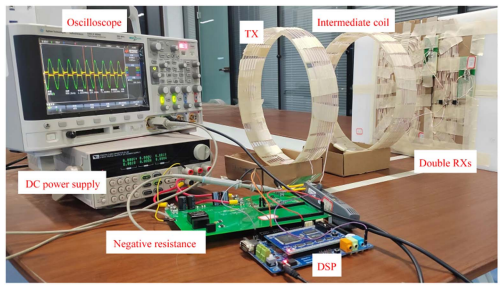

Fig. 13. Prototype of the proposed double-receiver pseudo-Hermitian WPT system incorporating an IC.

The steady operating frequency and its corresponding steady transfer efficiency can both be obtained by using the Simulink. If the steady operating frequency ω is very close to ω_0, the circulating current will be quite large, thus resulting in a low efficiency. As shown in Fig. 12(b), it is not recommended to use the system if the lateral misalignment may occur.

2) Nonzero-Cross-Coupling Between Double RXs: The evolution of the steady operating frequency and its corresponding steady transfer efficiency of the proposed system with a value k_{34} of 0.25, as a function of d, is shown in Fig. 12(d). In fact, the lateral misalignment performance depends on the coil shape and size, the value of k_{34}, the longitudinal distance D and the value of r_{load}. Thus, there is no universal conclusion and the lateral misalignment performance under each pair of parameters requires a specific analysis. Since double RXs are placed symmetrically is the assumption at the beginning of this research, a detailed analysis about the lateral misalignment can be made in the future.

As an improvement direction in the future, if IC is designed to generate a uniform magnetic field around the RXs, then the system is expected to be used under this scenario.

V. Experimental Verification

A. Experimental Prototype

A kind of 44AWG Litz wire consisting of 600 strands per turn is selected to wind the coils. The TX and IC are solenoid coils with a radius of 14.75 cm and 9 turns. The turn-to-turn distance is about 5.5 mm. The double RXs are both $29\text{cm} \times 16.5\text{cm}$ faced rectangular coils with 13 turns and a turn-to-turn distance of 4.5 mm. The prototype of the proposed system is shown in Fig. 13. The parameters of the coils selected in the experiment are measured by the network analyzer E4990A, as shown in Tables I and II. The natural resonant frequency of each coil is designed to be 1 MHz.

The locations of TX and IC are both fixed and they are coaxially placed. The center-to-center distance between TX and IC is fixed as 18.6 cm ($k_{12} = 0.0875$). The total transfer distance between TX and RX1/RX2 in the longitudinal direction is around 30–40 cm (determined by k_{23}). The relationship between k_{23} and the distance D is shown in Fig. 14. Note that D refers to the center-to-center distance between IC and RX1/RX2 in the longitudinal direction.

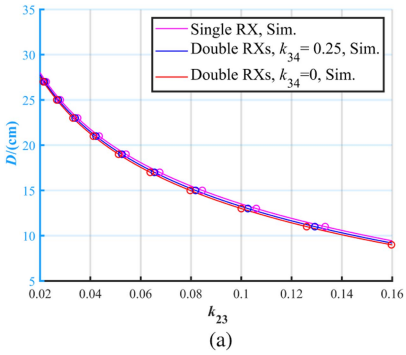

Fig. 14. Relationship between k_{23} and the distance D. For the proposed double-receiver system with a value k_{34} of $0/0.25$, RX1 and RX2 are not coaxially placed with IC. The center-to-center distance between RX1/RX2 with IC in the lateral direction is set as 4/3cm, respectively.

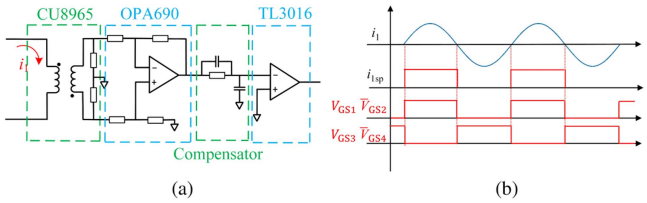

Fig. 15. Schematic diagram of the control circuit and the generation process of the feedback signal. (a) Schematic diagram of the control circuit. (b) Generation process of the feedback signal.

A full-bridge inverter-based negative resistance with a 15 V dc input is used to measure the steady transfer performance of the proposed system and the conventional system under different loads and transfer distances. For the pseudo-Hermitian WPT system operating in the normal operating state (i.e., the self-oscillating state), the input voltage V_{in} is always in phase of the input current i_1, thus at this time the full-bridge inverter can be equivalent as a negative resistance $-R$ and the zero-current-switching (ZCS) can be achieved.

The negative resistance $-R$ consists of a gallium nitride (GaN)-based full-bridge inverter (GS61008T) with two gate drivers Si8274, a current sensor CU8965, a difference amplifier OPA690, a phase compensator, a zero-crossing comparator TL3016 and a digital signal processor TMS320F28335. The GaN transistor GS61008T can operate at a high frequency with a low power loss. With the help of the ZCS operating and the desirable performance of GS61008T, the switching losses are limited.

A start-up strategy is used to ensure the reliable starting of the negative resistance. First, F28335 disables the feedback signal and ensures that the inverter is operating at the initial operating frequency ω_{ini}. Then, it disables the driven signal and enables the feedback signal to ensure that the inverter is operating in the self-oscillating state. The circuit diagram of a full-bridge inverter for realizing a negative resistance is shown in Fig. 2, while the control circuit is shown in Fig. 15(a) and the generation process of the feedback signal is shown in Fig. 15(b).

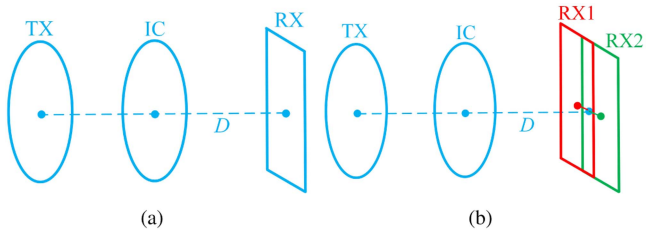

Fig. 16. Selected coil types of the conventional three-coil system and the proposed double-receiver system used in the experiment. (a) Conventional system. (b) Proposed system.

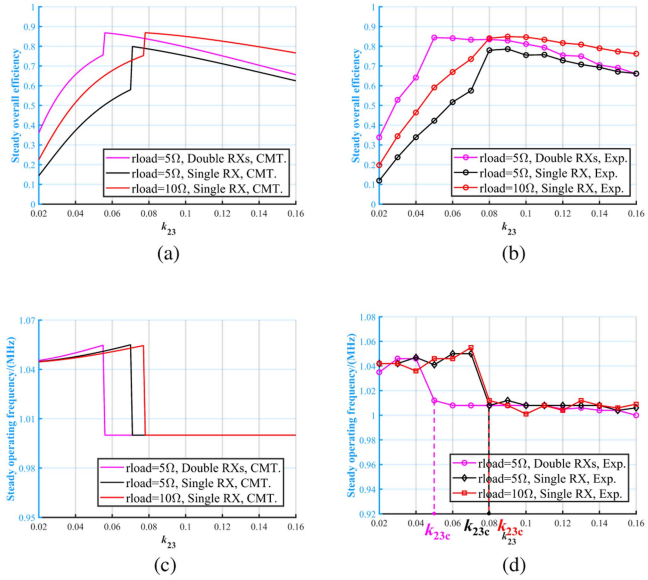

Fig. 17. Evolution of the steady overall efficiency and the steady operating frequency of the system as a function of the coupling coefficient k_{23}. Note that the steady overall efficiency refers to the DC–AC efficiency. Besides, in the experiment, the initial operating frequency ω_{ini} of the system is set as ω_0. The experimental results corresponding to three different situations are shown in Fig. 17, i.e., $r_{\text{load}} = 5/10\Omega$, Single RX and $r_{\text{load}} = 5\Omega$, Double RXs. (a) Effi., CMT. (b) Effi., Exp. (c) Freq., CMT. (d) Freq., Exp.

In order to demonstrate how the final structure is changed, the coil types of the conventional system and the proposed system are shown in Fig. 16(a) and (b), respectively.

B. Experimental Verification of the Advantages of the Proposed Double-Receiver Pseudo-Hermitian WPT System

1) Using Double Decoupled RXs to Extend the Strong-Coupling Region and Enhance the Steady Transfer Efficiency: The evolution of the steady overall efficiency and the steady operating frequency of the proposed double-receiver system with double decoupled RXs and the conventional three-coil system, under different loads, are shown in Figs. 17 and 18. It can be found that with the increase of k_{23}, a bifurcation will occur at the critical coupling coefficient $k_{23\text{c}}$.

In the weak-coupling region ($k_{23} < k_{23\text{c}}$), with the increase of k_{23}, the steady transfer efficiency will increase. While in the strong-coupling region ($k_{23} > k_{23\text{c}}$), with the increase of k_{23}, the steady transfer efficiency of the system will decrease. It is

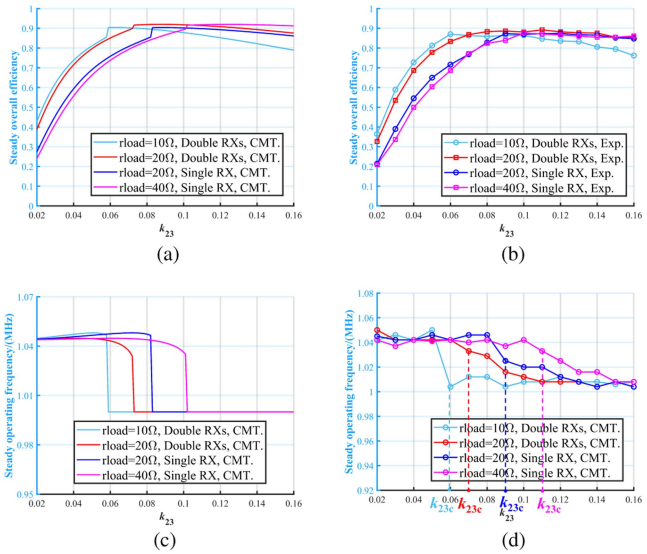

Fig. 18. Evolution of the steady overall efficiency and the steady operating frequency of the system as a function of the coupling coefficient k_{23}. Note that the steady overall efficiency refers to the DC–AC efficiency. Besides, in the experiment, the initial operating frequency $\omega_{\rm ini}$ of the system is set as ω_0. The experimental results corresponding to four different situations are shown in Fig. 18, i.e., $r_{\rm load} = 20/40\Omega$, Single RX and $r_{\rm load} = 10/20\Omega$, Double RXs. (a) Effi., CMT. (b) Effi., Exp. (c) Freq., CMT. (d) Freq., Exp.

obvious that for the conventional system with a 5Ω load, the evolution of the steady transfer efficiency is limited.

As shown in Fig. 17(d), with the increase of k_{23} as a step length of 0.01, the experimental results show that the critical coupling coefficient k_{23c} of the proposed system with a 5Ω load and the conventional system with the same 5Ω load are 0.05 and 0.08, respectively, thus the strong-coupling region is extended. In addition, as shown in Fig. 17(b), it can be found that for the conventional system with a low load coefficient, under the same load, using double decoupled RXs can enhance the steady transfer efficiency and extend the strong-coupling region.

Besides, as shown in Figs. 17(d) and 18(d), the experimental results demonstrate that for the proposed system with a $5/10/20\Omega$ load and the conventional system with a $10/20/40\Omega$ load, the value of critical coupling coefficient k_{23c} is $0.05/0.06/0.07$ and $0.08/0.09/0.11$, respectively. Thus, it can be concluded that the theoretical relationship between the critical coupling coefficients k_{23cs} and k_{23cd} under the same load coefficient (i.e., $k_{23cs} = \sqrt{2}k_{23cd}$) is consistent with the experimental results within the error range.

The steady operating waveform of the conventional system with a 5Ω load and a value k_{23} of 0.08 is shown in Fig. 19. With the increase of k_{23} as a step length of 0.01, a bifurcation will occur at $k_{23} = 0.08$ and a local maximum steady transfer efficiency (78.0%) is achieved. By using double decoupled RXs, under the same load, k_{23c} is reduced from 0.08 to 0.05 and a higher steady transfer efficiency is achieved in the weak-coupling region, as shown in Fig. 17(b). The maximum steady transfer efficiency is enhanced from 78% to 84.4%.

Six steady operating waveforms of the proposed system with double decoupled RXs and the conventional system are shown in

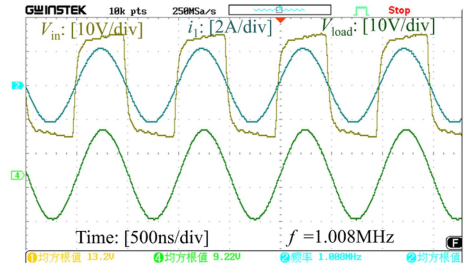

Fig. 19. Steady operating waveform of the conventional system with a 5Ω load and a value k_{23} of 0.08. $\eta = 78.0\%$, $K = 0.076{\rm W/V^2}$, $V_{\rm load}$ is 9.22 V and f is 1.008 MHz.

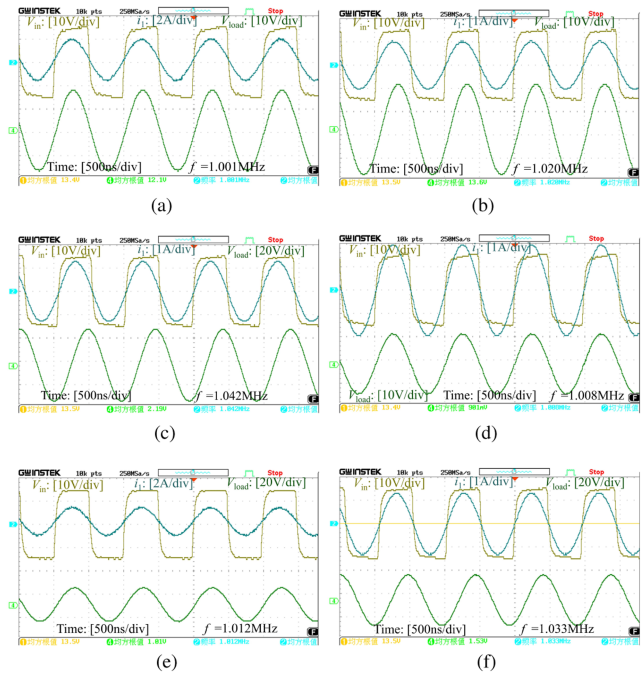

Fig. 20. Steady operating waveforms of the proposed system with double decoupled RXs and the conventional system under different situations. Note that the value of $\omega_{\rm ini}$ is set as 1 MHz. In (a), $V_{\rm load}$ is 12.1 V and f is 1.001 MHz; in (b), $V_{\rm load}$ is 13.6 V and f is 1.020 MHz; in (c), $V_{\rm load}$ is 21.9 V and f is 1.042 MHz; in (d), $V_{\rm load}$ is 9.01 V and f is 1.008 MHz; in (e), $V_{\rm load}$ is 10.1 V and f is 1.012 MHz; while in (f), $V_{\rm load}$ is 15.3 V and f is 1.033 MHz. (a) Single RX, $r_{\rm load} = 10\Omega$, $k_{23} = 0.10$, $\eta = 84.6\%$, $K = 0.065{\rm W/V^2}$. (b) Single RX, $r_{\rm load} = 20\Omega$, $k_{23} = 0.10$, $\eta = 87.0\%$, $K = 0.041{\rm W/V^2}$. (c) Single RX, $r_{\rm load} = 40\Omega$, $k_{23} = 0.10$, $\eta = 87.6\%$, $K = 0.053{\rm W/V^2}$. (d) Double RXs, $r_{\rm load} = 5\Omega$, $k_{23} = 0.07$, $\eta = 83.3\%$, $K = 0.072{\rm W/V^2}$. (e) Double RXs, $r_{\rm load} = 10\Omega$, $k_{23} = 0.07$, $\eta = 86.3\%$, $K = 0.045{\rm W/V^2}$. (f) Double RXs, $r_{\rm load} = 20\Omega$, $k_{23} = 0.07$, $\eta = 86.8\%$, $K = 0.052{\rm W/V^2}$.

Fig. 20. Experimental results demonstrate that for the proposed system and the conventional system under the same load coefficient, if $k_{23c} = \sqrt{2}k_{23d}$, then they have the same corresponding steady transfer efficiency and power conversion capability.

The distribution of the power losses of the system corresponding to different situations are shown in Fig. 21. The ohmic losses of the coupling coil and compensation capacitor are calculated by $P_{\rm r} = I^2 r$ and $P_{\rm ESR} = I^2 r_{\rm ESR}$, respectively. The power loss of the full-bridge inverter is obtained

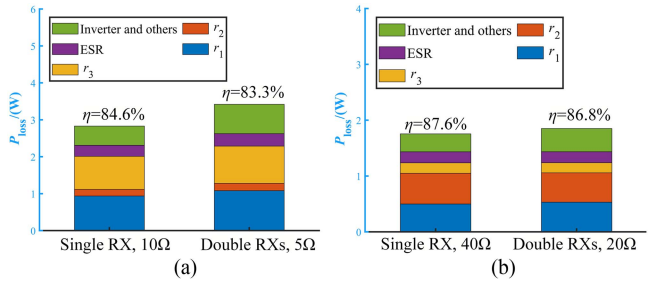

Fig. 21. Power losses calculation and distribution of the system. (a) Single RX, $r_{\text{load}} = 10\Omega$, $k_{23} = 0.10$ and double RXs, $r_{\text{load}} = 5\Omega$, $k_{23} = 0.07$. (b) Single RX, $r_{\text{load}} = 40\Omega$, $k_{23} = 0.10$ and double RXs, $r_{\text{load}} = 20\Omega$, $k_{23} = 0.07$.

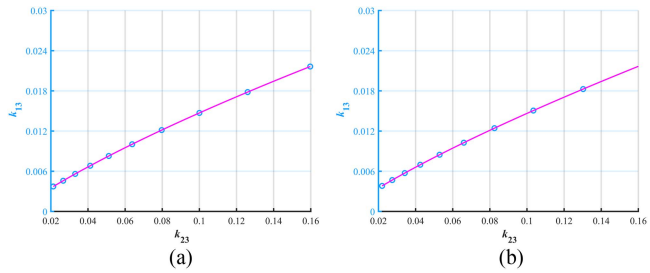

Fig. 22. Relationship between the coupling coefficients k_{23} and k_{13} under different values of k_{34} in the simulation. (a) $k_{34} = 0$. (b) $k_{34} = 0.35$.

by $P_{\text{inv}} = P_{\text{in}} - P_{\text{r}} - P_{\text{ESR}} - P_{\text{load}}$, where P_{in} is measured by the dc power supply directly. As shown in Fig. 21, for the proposed system and the conventional system under the same load coefficient, if $k_{23\text{c}} = \sqrt{2}k_{23\text{d}}$, the distributions of the power losses are almost the same, thus our conclusions in Section IV-A, Chapter IV have been verified.

It can be found from Figs. 17(d) and 18(d) that in the strong-coupling region, the experimental results demonstrate that the steady operating frequency will always higher than ω_0. This is caused by the existence of M_{13} and M_{14}. Although M_{13}/M_{14} between the TX and RX1/RX2 are small, they may still have an impact on the steady transfer performance of the system. By using the COMSOL Multiphysics, the relationship between the coupling coefficients k_{23} and k_{13}, under different values of k_{34}, are shown in Fig. 22.

To reveal the impact caused by k_{13}/k_{14}, by using Simulink, the evolution of the steady operating frequency and steady transfer efficiency of the proposed system with double decoupled RXs, without or after considering k_{13}/k_{14}, are shown in Fig. 23. Due to the existence of k_{13}/k_{14}, the steady operating frequency will always be higher than ω_0 in the strong-coupling region. Besides, the existence of k_{13}/k_{14} will have a negative impact on the steady transfer efficiency in the weak-coupling region.

In the experiment, when the system has been manufactured, the mutual inductance between the coupling coils may slightly differ from the theoretical predictions. In addition, the full-bridge inverter-based negative resistance used in the real world is not ideal. In conclusion, the differences are caused by the

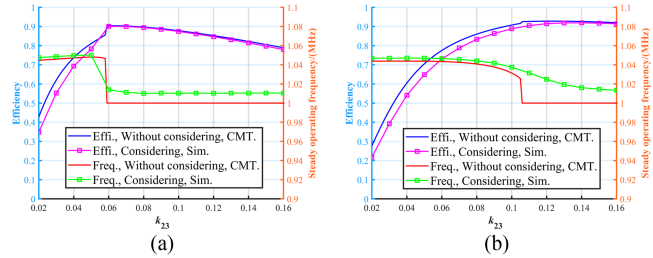

Fig. 23. Evolution of the steady transfer efficiency and steady operating frequency of the proposed system with double decoupled RXs, without or after considering k_{13} and k_{14}. Note that the value of ω_{ini} is set as 1 MHz. (a) $r_{\text{load}} = 10\Omega$. (b) $r_{\text{load}} = 40\Omega$.

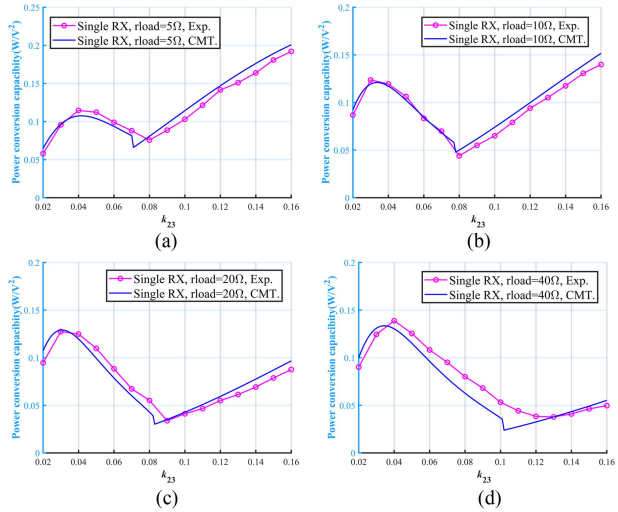

Fig. 24. Evolution of the power conversion capability of the conventional system as a function of k_{23} under different loads. Note that the value of ω_{ini} is set as 1 MHz. (a) $r_{\text{load}} = 5\Omega$. (b) $r_{\text{load}} = 10\Omega$. (c) $r_{\text{load}} = 20\Omega$. (d) $r_{\text{load}} = 40\Omega$.

existence of k_{13}/k_{14}, the manufacturing error and the power losses of the negative resistance $-R$.

2) Properly Setting the Cross-Coupling Between the Double RXs to Enhance the Power Conversion Capability: The evolution of the power conversion capability of the conventional system with different loads are shown in Fig. 24. It is obvious that the power conversion capability of the conventional system around the bifurcation point is low. To make a comparison, the evolution of the proposed system with double decoupled RXs under different loads are shown in Fig. 25(a), (c), and (e). Compared with the conventional system under the same load, using double decoupled RXs cannot enhance the power conversion capability in most cases.

As shown in Figs. 24 and 25(a), (c), and (e), it can be found that for the conventional system and the proposed system with double decoupled RXs, at the bifurcation point, the steady transfer efficiency of the system reaches its maximum while its power conversion capability reaches its minimum, thus resulting in a binary choice between the transfer efficiency and the output power.

Fortunately, by properly setting the cross-coupling between double RXs, the power conversion capability of the system can

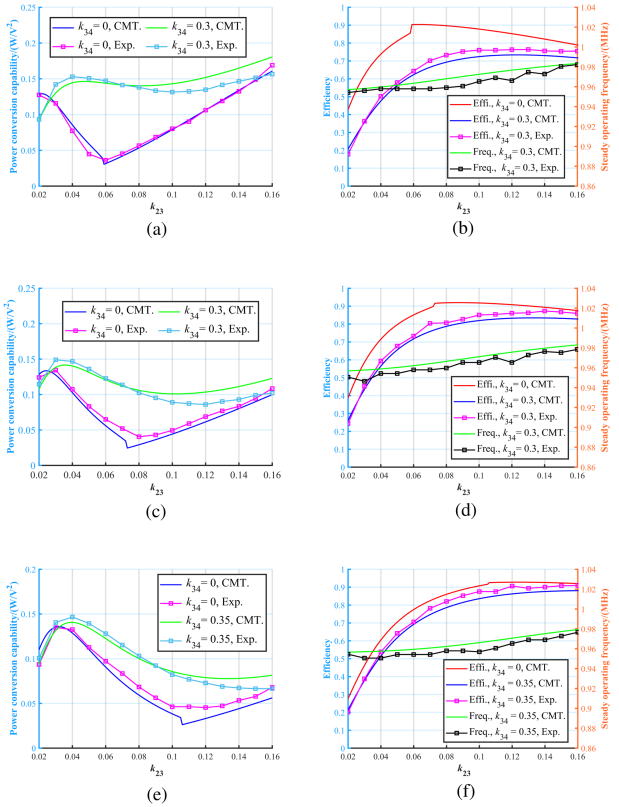

Fig. 25. Evolution of the power conversion capability, steady overall efficiency and steady operating frequency of the proposed system under different situations. Note that Pcc. is the abbreviation of the power conversion capability. In addition, for the proposed system with a value k_{34} of 0, the value of $\omega_{\rm ini}$ is set as 1 MHz. While for the proposed system with a value k_{34} of 0.3/0.35, $\omega_{\rm ini}$ is set as 0.949 MHz. (a) Pcc., $r_{\rm load} = 10\Omega$. (b) Effi. and Freq., $r_{\rm load} = 10\Omega$. (c) Pcc., $r_{\rm load} = 20\Omega$. (d) Effi. and Freq., $r_{\rm load} = 20\Omega$. (e) Pcc., $r_{\rm load} = 40\Omega$. (f) Effi. and Freq., $r_{\rm load} = 40\Omega$.

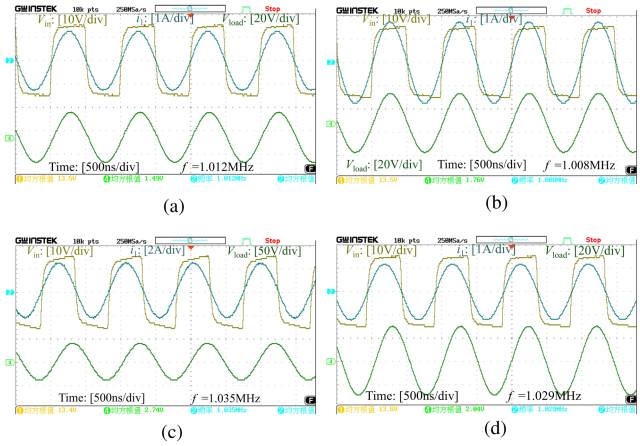

Fig. 26. Steady operating waveforms of the proposed system with double decoupled RXs under different situations. (a) and (b). $r_{\rm load} = 20\Omega$. (c) and (d). $r_{\rm load} = 40\Omega$. Note that the value of $\omega_{\rm ini}$ is 1 MHz. In (a), $V_{\rm load}$ is 14.9 V and f is 1.012 MHz; in (b) $V_{\rm load}$ is 17.6 V and f is 1.008 MHz; in (c) $V_{\rm load}$ is 27.4 V and f is 1.035 MHz, while in (d) $V_{\rm load}$ is 20.4 V and f is 1.029 MHz. (a) Double RXs, $r_{\rm load} = 20\Omega$, $k_{23} = 0.10$, $\eta = 88.1\%$, and $K = 0.049{\rm W/V^2}$. (b) Double RXs, $r_{\rm load} = 20\Omega$, $k_{23} = 0.12$, $\eta = 88.2\%$, and $K = 0.069{\rm W/V^2}$. (c) Double RXs, $r_{\rm load} = 40\Omega$, $k_{23} = 0.07$, $\eta = 81.9\%$, and $K = 0.083{\rm W/V^2}$. (d) Double RXs, $r_{\rm load} = 40\Omega$, $k_{23} = 0.10$, $\eta = 85.6\%$, and $K = 0.046{\rm W/V^2}$.

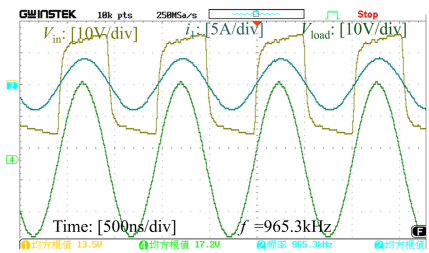

Fig. 27. Using the cross-coupling between the double RXs to enhance the power conversion capability. Note that $r_{\rm load} = 10\Omega$ and $k_{34} = 0.3$. $V_{\rm load}$ is 17.2 V and f is 965.3 kHz.

be enhanced, as shown in Fig. 25(a), (c), and (e). However, compared with the proposed system with double decoupled RXs, the enhancement of the power conversion capability of the system comes at a cost of the decrease in the steady transfer efficiency, as shown in Fig. 25(b), (d), and (f).

Therefore, a tradeoff between the enhancement of the power conversion capability of the system and the decrease in the steady transfer efficiency needs to be made. Fortunately, the experimental results reveal that this negative effect is slight if the load coefficient is not low. At this time a well-designed cross-coupling can be used to circumvent the binary choice between the transfer efficiency and the output power.

Four steady operating waveforms corresponding to the proposed system with double decoupled RXs under different situations are shown in Fig. 26. Besides, five steady operating waveforms corresponding to the proposed system with a nonzero value of k_{34} under different situations are shown in Figs. 27 and 28.

It can be found from comparing Figs. 27 with Fig. 20(a) that with the introduction of a value k_{34} of 0.3, the steady transfer efficiency is reduced from 84.6% to 76.0%, while the power conversion capability is enhanced from 0.065 to $0.132{\rm W/V^2}$. Besides, by comparing Fig. 28(b) with Fig. 20(b), it can be found that with the introduction of a value k_{34} of 0.3, the steady transfer efficiency is reduced from 87.0% to 85.1%, while the power conversion capability is enhanced from 0.041 to $0.089{\rm W/V^2}$.

In addition, by comparing Fig. 28(d) with Fig. 20(c), it is found that under the same 40Ω load, the decrease in the steady transfer efficiency caused by k_{34} is slight. With the use of a value k_{34} of 0.35, the power conversion capability of the system is enhanced from 0.053 to $0.082{\rm W/V^2}$, while the steady transfer efficiency almost remains unchanged.

Comparing Fig. 28(a) and (b) with Fig. 20(f) and 26(a), respectively, it can be found that compared with the proposed system with double decoupled RXs, the introduction of k_{34} will enhance the power conversion capability and have a negative impact on the steady transfer efficiency. Fortunately, by comparing Fig. 28(c) and (d) with Fig. 26(c) and (d), respectively, it can be found that this negative impact is slight if the value of $r_{\rm load}$ is high. Thus, the experimental results have verified our conclusions.

It is can be found from Fig. 25 that for the proposed system with a value k_{34} of 0.3/0.35, the steady overall efficiency will

TABLE III
COMPARISONS WITH THE EXISTING WPT SYSTEM WITH AN IC

Reference	Type	Frequency	Distance	Efficiency	Power	Restrictions
[2]	MCR	500kHz, fixed	2cm	up to 92%, DC-DC	changed with the charging process	M and ω are both fixed
[8]	PT	991kHz	42cm	91%, DC-AC, 15W in the PT-symmetric region		k_{23} must be equal to k_{12}
[9]	PT	86.8kHz	about 80cm	about 80%, DC-AC in the PT-symmetric region.		k_{23} must be equal to k_{12}
[10]	PT	400kHz	about 32cm	about 88%, DC-DC, 46W in the PT-symmetric region		k_{23} must be equal to k_{12}
[11]	PT	371.7kHz	30cm	about 85%, DC-DC, 48W in the PT-symmetric region		k_{23} must be equal to k_{12}
[19]	Pseudo-Hermitian	2MHz	about 8cm	up to about 85%, DC-AC	ungiven	As shown in this paper
[21]	Pseudo-Hermitian	200kHz	about 15cm	up to about 75%, DC-AC	5W in the strong-coupling region under the PI control	As shown in this paper
Our work	Pseudo-Hermitian	1MHz	about 40cm	up to about 90%, DC-AC	changed with k_{23} and r_{load}	Double RXs symmetrically placed

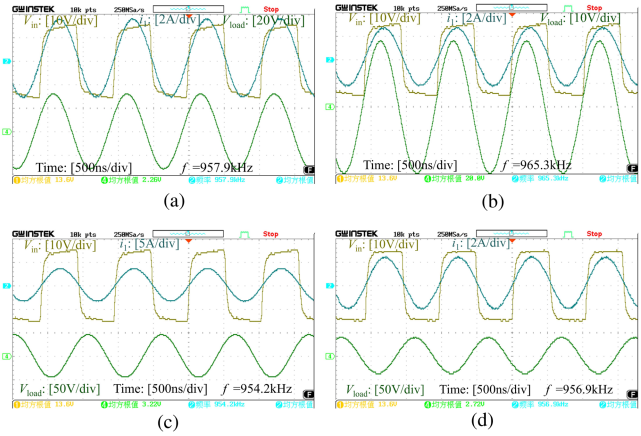

Fig. 28. Using the cross-coupling between the double RXs to enhance the power conversion capability. (a) and (b) $k_{34} = 0.3$ and $r_{\text{load}} = 20\Omega$. (c) and (d) $k_{34} = 0.35$ and $r_{\text{load}} = 40\Omega$. Note that the value of ω_{ini} is 0.949 MHz. In (a), V_{load} is 22.6 V and f is 957.9 kHz; in (b) V_{load} is 20 V and f is 965.3 kHz; in (c) V_{load} is 32.2 V and f is 954.2 kHz; while in (d) V_{load} is 27.2 V and f is 956.9 kHz. (a) Double RXs, $r_{\text{load}} = 20\Omega$, $k_{23} = 0.07$, $\eta = 80.4\%$, and $K = 0.114\text{W/V}^2$. (b) Double RXs, $r_{\text{load}} = 20\Omega$, $k_{23} = 0.10$, $\eta = 85.1\%$, and $K = 0.089\text{W/V}^2$. (c) Double RXs, $r_{\text{load}} = 40\Omega$, $k_{23} = 0.07$, $\eta = 78.2\%$, and $K = 0.115\text{W/V}^2$. (d) Double RXs, $r_{\text{load}} = 40\Omega$, $k_{23} = 0.10$, $\eta = 87.5\%$, and $K = 0.082\text{W/V}^2$.

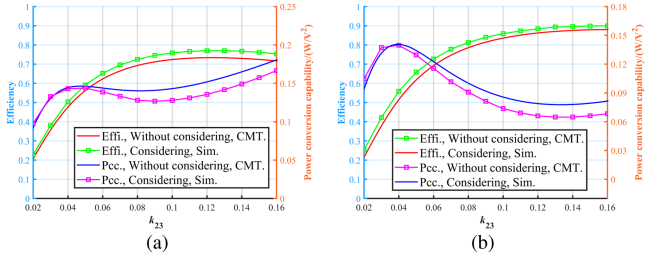

Fig. 29. Evolution of the steady transfer efficiency and power conversion capability of the proposed system with a nonzero value of k_{34}, without or after considering k_{13} and k_{14}. The value of ω_{ini} is set as 0.949 MHz. (a) $k_{34} = 0.3$, $r_{\text{load}} = 10\Omega$. (b) $k_{34} = 0.35$, $r_{\text{load}} = 40\Omega$.

be higher than the theoretical values. Besides, for the transfer region where k_{23} is not low, the power conversion capability of the system will lower than the theoretical value. These are also caused by the existence of k_{13}/k_{14}.

By using the Simulink, the evolution of the steady transfer efficiency and the power conversion capability of the proposed system with a nonzero value of k_{34}, without or after considering k_{13}/k_{14}, are shown in Fig. 29. Fig. 29 demonstrates that the existence of k_{13}/k_{14} is the main reason for the differences. The manufacturing error and the power loss of the negative resistance $-R$ are the other reasons for these differences.

C. Comparisons With the Existing WPT System With an IC

Table III compares the transfer performance of the existing WPT system with an IC reported in recent years. The key performance indices of their prototypes are listed in the table.

Previous work [2] proposes a load-independent WPT system with an IC. However, both the mutual inductance M between the coils and the operating frequency ω are assumed to be unchanged. These approximations make their work is not suitable for the application scenarios where the mutual inductance between the coils may change. In contrast, the novel pseudo-Hermitian WPT system proposed in this article can be used under the application scenarios where both the mutual inductance and the load may change.

For the three-coil PT WPT system consisting of a TX, an IC, and a RX proposed in [8], [9], [10], and [11], to ensure that the three-coil system is PT-symmetric, the coupling coefficient k_{23} must be equal to the coupling coefficient k_{12}, which generally requires a precise mechanical control of the system. However, such a rigid restriction is not needed for the pseudo-Hermitian WPT system.

For the conventional three-coil pseudo-Hermitian WPT system studied in[19] and [21], it still has two limitations, as illustrated in this article. Compared with the conventional three-coil system, the proposed double-receiver system incorporating an IC is expected to overcome these limitations.

VI. CONCLUSION

In this article, a novel double-receiver pseudo-Hermitian WPT system incorporating an IC is proposed. The CMT model is used to evaluate the advantages of the proposed double-receiver system compared with a conventional three-coil pseudo-Hermitian system. The major contributions of this article are given as follows:

1) It is first shown that with series-compensation coils, the conventional system has two limitations. One is it exhibits

a limited steady transfer efficiency under a low load coefficient, the other is if a full-bridge inverter is used to implement the negative resistance, the output power reaches its minimum at the bifurcation point with a maximum transfer efficiency.

2) It is found that if the load coefficient of the conventional system is low, using the proposed system with double decoupled RXs can extend the strong-coupling region and enhance the steady transfer efficiency under the same load.
3) It is found that a well-designed cross-coupling between the double RXs can be used to enhance the power conversion capability, thus circumventing the binary choice between the steady transfer efficiency and the output power.

Experimental results have validated our contributions. By using double decouple RXs, the strong-coupling region can be extended and the steady transfer efficiency can be enhanced under the same 5/10Ω load. Experimental results also show that by leveraging the cross-coupling between the double RXs, a few times enhancement in the power conversion capability can be achieved under the same 10/20/40Ω load.

Appendix A

The expressions of the coefficients c_5, c_4, c_3, c_2, c_1, and c_0 are shown in (13) in detail

$$
\begin{aligned}
c_5 &= -(1+k_{34})^2 \\
c_4 &= -k_{34}(1+k_{34}) \\
c_3 &= 2\left(\Gamma_{20}\Gamma_{30}+\frac{1}{2}k_{23}^2\right)(1+k_{34})-\frac{1}{4}k_{34}^2+\frac{1}{4}k_{12}^2(1+k_{34})^2 \\
&\quad -(\Gamma_{20}\Gamma_{30}+\Gamma_{20}k_{34})^2 \\
c_2 &= k_{34}\left(\Gamma_{20}\Gamma_{30}+\frac{1}{2}k_{23}^2\right)+\frac{1}{4}k_{12}^2k_{34}(1+k_{34}) \\
&\quad -\Gamma_{20}k_{34}(\Gamma_{20}+\Gamma_{30}+\Gamma_{20}k_{34}) \\
c_1 &= -\left(\Gamma_{20}\Gamma_{30}+\frac{1}{2}k_{23}^2\right)^2+\frac{1}{16}k_{12}^2k_{34}^2-\frac{1}{4}k_{12}^2(1+k_{34}) \\
&\quad \times\left(\Gamma_{20}\Gamma_{30}+\frac{k_{23}^2}{2}\right)-\frac{1}{4}\Gamma_{20}^2k_{34}^2 \\
&\quad +\frac{1}{4}k_{12}^2\Gamma_{30}(\Gamma_{20}+\Gamma_{30}+\Gamma_{20}k_{34}) \\
c_0 &= -\frac{1}{8}k_{12}^2k_{34}\left(\Gamma_{20}\Gamma_{30}+\frac{k_{23}^2}{2}\right)+\frac{1}{8}k_{12}^2k_{34}\Gamma_{20}\Gamma_{30}. \qquad (13)
\end{aligned}
$$

Appendix B

In Appendix B, some qualitative experience about the design of the proposed system is demonstrated. First, the variation range of load resistance and the permitted position of the coil should be clarified. Then, determine whether the conventional three-coil system can be used. If the answer is negative, clarify whether the proposed system can meet the requirement. Does it fall under the two limitations of the conventional system? Can double RXs be symmetrically placed about IC?

Third, determine the selected coil type of the double RXs. For the proposed system, the noncoaxial placement between IC and RX1/RX2 will reduce k_{23}/k_{24}.A reasonable coil type should ensure that this negative impact is slight.

Finally, determine the selected coil parameters by using the derivations shown in Chapter II. Currently, the trial-and-error method is used in our work. As an improvement in the future, the optimization algorithms can be used.

References

[1] A. Kurs et al., "Wireless power transfer via strongly coupled magnetic resonances," *Science*, vol. 317, no. 5834, pp. 83–86, Jul. 2007.

[2] Y. Li et al., "Reconfigurable intermediate resonant circuit based WPT system with load-independent constant output current and voltage for charging battery," *IEEE Trans. Power Electron.*, vol. 34, no. 3, pp. 1988–1992, Mar. 2019.

[3] X. Li, J. Hu, H. Wang, X. Dai, and Y. Sun, "A new coupling structure and position detection method for segmented control dynamic wireless power transfer systems," *IEEE Trans. Power Electron.*, vol. 35, no. 7, pp. 6741–6745, Jul. 2020.

[4] Y. Lim, H. Tang, S. Lim, and J. Park, "An adaptive impedance-matching network based on a novel capacitor matrix for wireless power transfer," *IEEE Trans. Power Electron.*, vol. 29, no. 8, pp. 4403–4413, Aug. 2014.

[5] T. Diekhans and R. W. De Doncker, "A dual-side controlled inductive power transfer system optimized for large coupling factor variations and partial load," *IEEE Trans. Power Electron.*, vol. 30, no. 11, pp. 6320–6328, Nov. 2015.

[6] S. Assawaworrarit, X. Yu, and S. Fan, "Robust wireless power transfer using a nonlinear parity-time-symmetric circuit," *Nature*, vol. 546, no. 7658, pp. 387–390, Jun. 2017.

[7] C. M. Bender and S. Boettcher, "Real spectra in non-Hermitian Hamiltonians having PT symmetry," *Phys. Rev. Lett.*, vol. 80, pp. 5243–5246, Jun. 1998.

[8] X. Shu, B. Zhang, Z. Wei, C. Rong, and S. Sun, "Extended-distance wireless power transfer system with constant output power and transfer efficiency based on parity-time-symmetric principle," *IEEE Trans. Power Electron.*, vol. 36, no. 8, pp. 8861–8871, Aug. 2021.

[9] C. Zeng et al., "High-order parity-time symmetric model for stable three-coil wireless power transfer," *Phys. Rev. Appl.*, vol. 13, Mar. 2020, Art. no. 034054.

[10] Y. Yue, J. Yang, and R. Li, "A three-coil constant output wireless power transfer system based on parity–time symmetry theory," *Appl. Sci.*, vol. 13, no. 22, Nov. 2023, Art. no. 12188.

[11] Y. Qu, B. Zhang, W. Gu, and X. Shu, "Wireless power transfer system with high-order compensation network based on parity-time-symmetric principle and relay coil," *IEEE Trans. Power Electron.*, vol. 38, no. 1, pp. 1314–1323, Jan. 2023.

[12] Y. Gu, J. Wang, Z. Liang, and Z. Zhang, "A wireless in-flight charging range extended PT-WPT system using S/Single-inductor-double-capacitor compensation network for drones," *IEEE Trans. Power Electron.*, vol. 38, no. 10, pp. 11847–11858, Oct. 2023.

[13] Y. Gu, Q. Zhu, L. Jia, G. Li, and Z. Zhang, "Optimized high-order compensation topology for PT-WPT systems with expanded constant power region," *IEEE Trans. Magn.*, vol. 59, no. 11, Nov. 2023, Art. no. 8203306.

[14] H. Chen, D. Qiu, C. Rong, and B. Zhang, "A double-transmitting coil wireless power transfer system based on parity time symmetry principle," *IEEE Trans. Power Electron.*, vol. 38, no. 11, pp. 13396–13404, Nov. 2023.

[15] L. Wu, B. Zhang, and J. Zhou, "Efficiency improvement of the parity-time-symmetric wireless power transfer system for electric vehicle charging," *IEEE Trans. Power Electron.*, vol. 35, no. 11, pp. 12497–12508, Nov. 2020.

[16] S. Sun, B. Zhang, C. Rong, X. Shu, and Z. Wei, "A multireceiver wireless power transfer system using self-oscillating source composed of zero-voltage switching full-bridge inverter," *IEEE Trans. Ind. Electron.*, vol. 69, no. 3, pp. 2885–2895, Mar. 2022.

[17] Y. Gu, J. Wang, Z. Liang, and Z. Zhang, "Flexible constant-power range extension of self-oscillating system for wireless in-flight charging of drones," *IEEE Trans. Power Electron.*, vol. 39, no. 11, pp. 15342–15355, Nov. 2024.

[18] J. Liu, X. Qu, Y. Li, and C. Ma, "Investigation of PT-symmetric frequency and compensation for IPT coupling-independent CC/CV and efficiency in wide load range," *IEEE Trans. Power Electron.*, vol. 38, no. 11, pp. 13353–13362, Nov. 2023.
[19] X. Hao et al., "Frequency-stable robust wireless power transfer based on high-order pseudo-Hermitian physics," *Phys. Rev. Lett.*, vol. 130, Feb. 2023, Art. no. 077202.
[20] A. Mostafazadeh, "Pseudo-Hermiticity versus PT symmetry: The necessary condition for the reality of the spectrum of a non-Hermitian hamiltonian," *J. Math. Phys.*, vol. 43, no. 1, pp. 205–214, Jan. 2002.
[21] Z. Zhang et al., "Communication-free robust wireless power transfer with constant output power and stable frequency," *Phys. Rev. Appl.*, vol. 23, Jan. 2025, Art. no. 014029.
[22] C. Zeng et al., "Efficient and stable wireless power transfer based on the non-Hermitian physics," *Chin. Phys. B*, vol. 31, no. 1, Jan. 2022, Art. no. 010307.
[23] R. I. Leine and H. Nijmeijer, *Dynamics and Bifurcations of Non-Smooth Mechanical Systems*. Berlin, Germany: Springe, 2004.
[24] A. El Aroudi, L. Benadero, E. Ponce, C. Olalla, F. Torres, and L. Martínez-Salamero, "Nonlinear dynamic modeling and analysis of self-oscillating H-bridge parallel resonant converter under zero current switching control: Unveiling coexistence of attractors," *IEEE Trans. Circuits Syst. I: Reg. Papers*, vol. 66, no. 4, pp. 1657–1667, Apr. 2019.
[25] Z. Zhu et al., "Efficiency optimization and power allocation of omnidirectional wireless power transfer for multiple receivers," *IEEE Trans. Ind. Electron.*, vol. 70, no. 10, pp. 9689–9699, Oct. 2023.

Zhijiang Liang was born in Liaoning, China, in 1998. He received the B.S. degree in electrical engineering in 2020, from Xi'an Jiaotong University, Xi'an, China, in 2020, where he is currently working toward the Ph.D. degree in electrical engineering.

His research interests include non-Hermitian theory, wireless power transfer, and automatic control.

Lihui Yang received the Ph.D. degree in electrical engineering from Xi'an Jiaotong University, Xi'an, China, in 2010.

From 2008 to 2009, she was a Visiting Ph.D. Student with the Centre for Electric Technology, Technical University of Denmark, Kongens Lyngby, Denmark. During June–October 2010, she was a Research Assistant with the Department of Electrical Engineering, Hong Kong Polytechnic University, Hong Kong. She is currently an Associate Professor with Xi'an Jiaotong University. Her research interests include stability and control of renewable energy conversion systems.

Xianglin Hao (Student Member, IEEE) was born in 1998. He received the bachelor's and master's degrees in electrical engineering from Xi'an Jiaotong University, Xi'an, China, in 2020 and 2023, respectively. He is currently working toward the Ph.D. degree in electrical engineering with the City University of Hong Kong, Hong Kong.

His research interests include non-Hermitian theory, wireless power transfer, and power amplifiers.

Mr. Hao is as a Student Member of CIGRE.

Chaoran Yang was born in Anhui, China, in 1998. He received the B.Sc. degree in measurement and control technology and instrument from the Hefei University of Technology, Hefei, China, in 2020. He is currently working toward the Ph.D. degree in electrical engineering with Xi'an Jiaotong University, Xi'an, China.

His main research interests include design and application of power electronic technology.

Shiqing Cai (Student Member, IEEE) was born in 1999. He received the B.Sc. degree in electrical engineering from Jilin University, Jilin, China, in 2021. He is currently working toward the Ph.D. degree in electrical engineering with Xi'an Jiaotong University, Xi'an, China.

His research interests include resonant converters, non-Hermitian theory, and wireless power transfer systems.

Xikui Ma was born in Shaanxi, China, in 1958. He received the B.Sc. and M.Sc. degrees in electrical engineering from Xi'an Jiaotong University, Xi'an, China, in 1982 and 1985, respectively.

In 1985, he joined as a Lecturer with the Faculty of Electrical Engineering, Xi'an Jiaotong University, where he became a Professor in 1992. He has authored or coauthored more than 270 scientific and technical papers, and also authored 12 books on electromagnetic fields and power electronics. His research interests include numerical methods in solving electromagnetic problems and the applications of digital control to power electronics.

Mr. Ma was the recipient of the best paper award for COMPEL 2021.